REVISTA
SOCIEDAD CIENTÍFICA DEL PARAGUAY

ISSN 0379-9123 • e-ISSN 2617-4731
Volumen 30 Número 01 • enero-junio 2025
Doi: https://doi.org/10.32480/rscp.2025.30.1.4455
Páginas de 44 a 55
Recibido: 04/02/2025 • Aceptado: 20/03/2025
Editor: Luis Dávalos Dávalos

Original Article
Artículo Original

BIOMIMETIC COATING OF ALUMINA SCAFFOLDS AT DIFFERENT IMMERSION TIMES
RECUBRIMIENTO BIOMIMÉTICO DE ANDAMIOS DE ALÚMINA EN DIFERENTES TIEMPOS DE INMERSIÓN

Crislayne G. Andreto
Mechanical and Industrial Engineering Department, Federal University of São João Del Rei (UFSJ)
São João Del Rei, Brazil.
Orcid: https://orcid.org/0000-0001-8098-5353
Mikhael Rodarte
Mechanical and Industrial Engineering Department, Federal University of São João Del Rei (UFSJ)
São João Del Rei, Brazil.
Orcid: https://orcid.org/0009-0004-9453-4923
Roseli M. Balestra
Mechanical and Industrial Engineering Department, Federal University of São João Del Rei (UFSJ)
São João Del Rei, Brazil.
Orcid: https://orcid.org/0000-0001-9968-3187
Lais S. Alves
Division of Materials, National Institute of Technology
Rio de Janeiro, Brazil
Orcid: https://orcid.org/0000-0003-0541-1151
Alexandre A. Ribeiro
Division of Materials, National Institute of Technology
Rio de Janeiro, Brazil.
Orcid: https://orcid.org/0000-0002-5299-4241
Magna Monteiro
Bio and Materials Laboratory, Polytechnic School, National University of Asunción.
San Lorenzo, Paraguay.
Orcid: https://orcid.org/0000-0002-5078-7214
***Autor corresponsal**: Magna Monteiro: mmonteiro@pol.una.py*

Cómo citar este artículo:
Andreto C, Rodarte M, Balestra R, Alves L, Ribeiro A, Monteiro M. Biomimetic coating of alumina scaffolds at different immersion times. Rev. Soc. cient. Parag. 2025;30(1): 44-55.

ABSTRACT
The biomimetic method can be used to coat scaffolds with calcium phosphate to improve bioactivity. This method presents the advantages of low cost, reproducibility, and applicability to complex surface and porous structures. This study aimed to manufacture alumina scaffolds coated with calcium phosphate by a biomimetic method for use as a biomaterial. The scaffolds were compacted at 200 MPa with 40 wt.% ammonium bicarbonate and 60 wt.% alumina, subjected to heat treatment at 270 °C for 120 min, and sintered at 1500 °C for 120 min. The samples were biomimetically coated by immersing them in a simplified solution of calcium chloride dihydrate (CaCl2.2H2O) and sodium hydrogen phosphate dihydrate (Na2HPO4.2H2O) for 7, 14, and 21 days. The samples were characterized by Archimedes' principle for density and porosity determination, Scanning Electron Microscopy (SEM), Energy Dispersive Spectroscopy (EDS), X-ray diffraction (XRD), and Fourier-transform infrared (FTIR). The scaffolds showed a porosity of 55%, with homogeneous distribution, interconnection, and pore sizes. Calcium phosphate formation was observed on the scaffold surfaces after 21 days of biomimetic coating. The samples presented promising results for use as biocompatible scaffolds.
Keywords: Scaffold; Alumina; Biomimetic coating; Bioceramics; Porosity.

RESUMEN
El método biomimético se puede utilizar para recubrir andamios con fosfato cálcico para mejorar la bioactividad. Este método tiene las ventajas de bajo costo, reproducibilidad y aplicabilidad a superficies complejas y estructuras porosas. Este estudio tuvo como objetivo fabricar andamios de alúmina recubiertos de fosfato de calcio utilizando un método biomimético para su uso como biomaterial. Los andamios se compactaron a 200 MPa con 40% en peso de bicarbonato de amonio y 60% en peso de alúmina, se trataron térmicamente a 270 °C durante 120 min y se sinterizaron a 1500 °C durante otros 120 min. Las muestras se recubrieron biomiméticamente, sumergiéndolas en una solución simplificada de cloruro de calcio dihidrato (CaCl2.2H2O) e hidrogeno fosfato de sodio dihidrato (Na2HPO4.2H2O) durante 7, 14 y 21 días. Las muestras se caracterizaron utilizando el principio de Arquímedes para la determinación de densidad y porosidad, microscopía electrónica de barrido (SEM), espectroscopia de energía dispersiva (EDS), difracción de rayos X (XRD) e infrarrojo con transformada de Fourier (FTIR). Los andamios presentaron una porosidad del 55%, con distribución, interconexión y tamaños de poro homogéneos. Se observó formación de fosfato de calcio en las superficies del andamio después de 21 días de recubrimiento biomimético. Las muestras presentaron resultados prometedores para su uso como andamios biocompatibles.
Palabras clave: Andamio; Alúmina; Recubrimiento biomimético; Biocerámica; Porosidad.

INTRODUCTION

The increase in life expectancy associated with advances in the healthcare industry leads to a problematic cycle in countries considered elderly—the increase in the elderly increases related diseases, such as bone tissue diseases (osteoporosis). In addition, fractures in bone tissue can occur in many ways, such as accidents, diseases, and tumors. For this reason, advanced research in biomaterials is conducted to address the growing demands of the healthcare system [1,2].

Biomaterials are designed to repair or replace parts of the biological system. They must interact with tissues and organs, over an extended period, performing specific functions to temporarily or permanently reconstruct damaged body parts. Tissue regeneration applications should satisfy biocompatibility, bioactivity, osteoconductivity, and porosity integration [3,4].

Ceramic materials have been extensively used in medicine due to their biocompatibility, high stiffness, and compression strength, which make them ideal for orthopedic implant applications [5-7]. The most well-known ceramics in biomedical applications are alumina (Al2O3), calcium phosphates, and their different phases.

Bone tissue consists of approximately 65% inorganic phases, mainly calcium phosphate (CaP). This phase, primarily composed of hydroxyapatite (HA, $Ca_{10}(PO_4)_6(OH)_2$), provides rigidity and strength [8]. Calcium phosphates and hydroxyapatites are ceramics that can be synthesized by a biomimetic coating, for example. These ceramics can be biocompatible, bioabsorbable, osteoinductive, and thermally stable; therefore, they are suitable for temporary applications where the implant is replaced by new tissue [7,9-11]. On the other hand, alumina (Al_2O_3) is a widely used commercial bioinert ceramic with high compressive strength, and it is extensively used in applications that require resistance to mechanical stress[12-14].

Scaffolds are structures composed of interconnected pores of different sizes. Within biological systems, scaffolds enable the flow of body fluids, which transport nutrients that activate the osteoinduction mechanism, favoring osteoconduction and osseointegration. Together, these processes promote the adhesion and differentiation of the bone cells [15,16]. When cells with osteogenic potential come into contact with an appropriate biomaterial, tissue regeneration can occur. Therefore, the interaction between the implant and the body proteins is fundamental to the material's biocompatibility [17]. Porous alumina bone implants have shown excellent osseointegration results, combining strong implant-tissue interaction, outstanding mechanical properties [3,18], and good cell growth and adhesion within pores observed *in vivo* studies [17,19].

A bioactive coating can be applied to the surface of the bioinert implant to enhance the scaffold's biological response and improve the implant-bone interaction. Abe et al. proposed a widely recognized method to coat bioinert surfaces, and it has been used and refined over time [20]. This method involves immersing the scaffold in a solution resembling body fluid, called Simulated Body Fluid (SBF), for an adequate period to induce calcium phosphate deposition. The biomimetic method presents numerous advantages over others, such as deposition on porous surfaces and complex

geometries, as well as producing homogeneous coatings, with the formation of hydroxyapatite crystals at low temperatures and low cost [21-23]. Promising results are reported in the literature on procedures performed for up to 21 days[18,22,24].

This research aimed to deposit a bioactive calcium phosphate layer on alumina scaffolds with structural, chemical, and physical properties suitable for application in bone regeneration. The samples were processed with interconnected pores, which made them biologically functional. To achieve this, the quantity and size of the pores were controlled, varying the amount of the pore-forming agent. The biomimetic method was applied to coat the scaffolds with calcium phosphate, obtaining a bioactive layer on both the surface and within the pores.

EXPERIMENTAL PROCEDURE

The scaffolds were produced using commercial alumina powder (CT 3000 SG, Almatis In., 0.8 µm) and alimentary-grade ammonium bicarbonate (NH_4HCO_3) (Art Alimentos, 250-425 µm) as a pore-forming agent.

The scaffolds manufactured by powder metallurgy were prepared from the mixture of alumina and the pore-forming agent 60 and 40% (wt./wt.), respectively. They were mixed manually in polypropylene containers for 1 min. Then, the mixture was compacted under uniaxial pressure (200 MPa) for 1 min in a tempered steel cylindrical die of 10 mm in diameter. Samples were heat-treated to remove the pore-forming agent at 270 °C, with heating and cooling rates of 1 °C/min for 120 min. After this, samples were sintered at 1500 °C for 120 min. The sample was manually sanded to remove the first surface layer to observe the scaffolds and evaluate the porosity, pore shape, and interconnection.

For the biomimetic coating process, the Synthetic Body Fluid Simplified Solution (SS) with pH 7.0 was prepared from calcium chloride dehydrate ($CaCl_2.2H_2O$) and sodium hydrogen phosphate dehydrate ($Na_2HPO_4.2H_2O$) dissolved separately in distilled water under magnetic stirring for 10 minutes. The ionic concentration of SBF is presented in Table 1.

Na^+	K^+	Mg^{+2}	Ca^{+2}	Cl^-	HCO_3^-	HPO_4^{-2}	SO_4^{-2}
142,00	5,00	1,50	2,50	147,80	4,20	1,00	0,05

Table 1. *SBF ionic concentration.*

The scaffolds were immersed in the SS for 7, 14, and 21 days; after two days, a new solution was prepared and renewed during the assay. After these periods, the biomimetically coated samples were washed with distilled water and dried at 37 °C for 24 h to remove excess moisture from the surface[20,22]. The immersion time in the SBF was the parameter used to name the samples: 0B – no biomimetic coating or 0 days in immersion; 7B – 7 days of immersion; 14B – 14 days of immersion; 21B – 21 days of immersion.

The density (Eq. 1), relative density (Eq. 2), and porosity (Eq. 3) of the alumina scaffolds were determined by the Archimedean density principle. The samples were weighed using an analytical balance with a density determination kit, and their diameter and height were measured at 3 points using a caliper.

$$\boldsymbol{\rho = \frac{m}{\pi \frac{D^2}{4} . h}} \quad (1)$$

$$\boldsymbol{\delta = \frac{\rho}{\rho_{Al}} . 100} \quad (2)$$

$$\boldsymbol{\%pores = 100 - \delta} \quad (3)$$

Where m is the mass of the samples; D is the diameter of the samples; h is the thickness of the samples; δ is the relative density; ρ_{Al} is the theoretical density of alumina (3.95 g/cm³).

The samples were analyzed before and after the biomimetic assays to assess the evolution of calcium phosphate layer formation at different immersion times. The porous samples were analyzed using scanning electron microscopy coupled with an energy-dispersive X-ray spectrometer (SEM-EDS; Zeiss EVO-15) to characterize their surface structure, pore size, distribution, and interconnection during the deposition of the biomimetic coating. For the SEM morphology analysis, the samples were coated with Au (20 µA and thickness of 10 nm). In contrast, for EDS monitoring of calcium phosphate layer formation, they were coated with C (20 µA and thickness of 10 nm). The pores were measured using the free software ImageJ.

Crystalline phases were identified by X-ray powder diffraction (X'Pert³, Malvern Panalytical, Netherlands) with CuKα radiation at 40 kV and 40 mA, 2θ range 5 – 80°, speed step size 0.5°/min, and time step 2.0 s. The Fourier-transform infrared-FTIR spectrometer Nicolet iS5 (ThermoScientific, U.S.) was used to identify the functional groups' vibrational mode characteristics. A thin layer of the material was removed, and the samples were prepared using the KBr pellets technique. Then, spectra between 400 and 4000 cm^{-1} were recorded, with a resolution of 4 cm^{-1} and 128 scans per sample.

RESULTS AND DISCUSSION

Density and porosity

Table 2 shows the density, relative density, and porosity obtained by the Archimedean method before (0B) and after the biomimetic coating (7B, 14B, and 21B).

Samples	Density (g/cm^3)	Relative density (%)	Porosity (%)	Porosity Standard deviation
0B	1.77	44.7	55.3	0.4761
7B	1.76	44.6	55.4	0.3852
14B	1.76	44.5	55.5	0.2527
21B	1.77	44.9	55.1	0.5577

Table 2. *Density, relative density, and porosity of the scaffolds.*

According to Table 2, it is possible to affirm that the biomimetic method did not show significant changes in the density, relative density, and porosity values. However, a slight increase in these parameters is observed in the 21B sample, which could be attributed to the thickness of the deposited layer. Regarding the density and relative density of the 0B sample, the differences observed in the other samples could be related to the potential dissolution or release of particles into the solution. It was anticipated that the biomimetic coating would not reduce the porosity on the scaffold[21,23,25,26].

Microstructural, chemical, and morphological analysis

Figure 1 presents the SEM micrographs of the scaffolds before the biomimetic coating. Microscopy of sanded samples (Figure 1b) reveals the presence of open and interconnected pores, which are essential characteristics for scaffold functionality. Compared to the non-sanded samples (Figure 1a), the sanded samples exhibit more exposed pores due to removing the layer formed during the compaction process, which obstructs the pores and may limit their interconnectivity, as seen in Figure 1a.

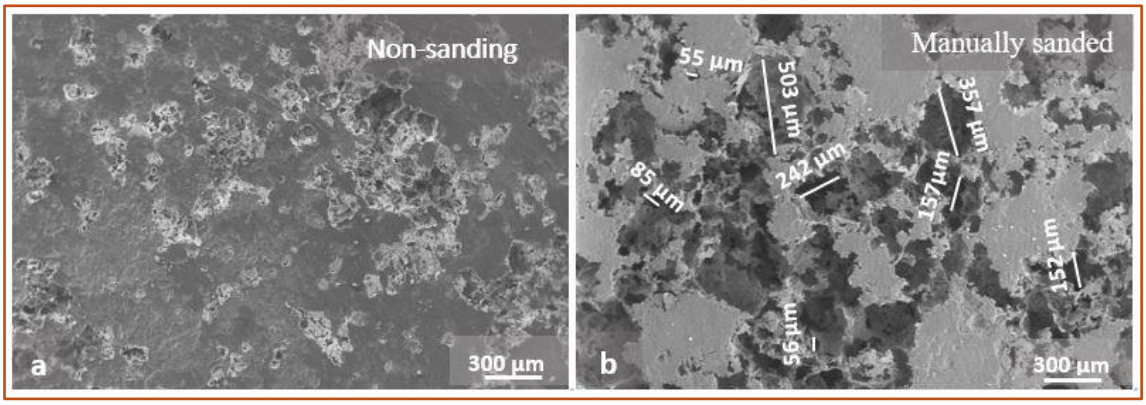

Figure 1. *SEM of scaffold surfaces before the biomimetic coating: a) non-sanded; b) manually sanded. 100x.*

Figure 1b shows pores of different sizes in a vast, broad, and expected range (50-600 µm). In general, scaffolds with larger pores have thinner walls, which reduces the mechanical strength. Micropores smaller than 50 µm can favor cell transport and bone growth by enhancing the surface area for protein absorption, promoting osteoblast adhesion, and developing the capillary system inside pores. However, pore sizes between 100-600 µm are crucial to improve the biological activity of implants used in bone tissue replacement and restoration. Osteoblast growth was noticed in pores between 380-405 µm, fibroblasts between 186-200 µm, and bone tissue between 290-310 µm. Pores greater than 200 µm and smaller than 100 µm are essential to osteoconductivity[18,19,27,28].

Figure 2 presents the evolution of the calcium phosphate layer growth during the biomimetic process, comparing the samples before (0 days) and after 7, 14, and 21 days of immersion. In Figure 2b, seven days of immersion may induce calcium and phosphorus formation on the samples' surface. While the SEM images clearly show the presence of these elements at 14 and 21 days, they are not evident in the SEM images at 7 days. However, the calcium and phosphorus content are confirmed by EDS analysis. As the red arrows indicate, extending the immersion time to 14 days allows for observing nucleation points corresponding to the phosphate deposition. As the immersion time increased, it was possible to observe the growth of the calcium phosphate layer on the samples. After 21 days, the samples presented a uniform coating across the entire surface.

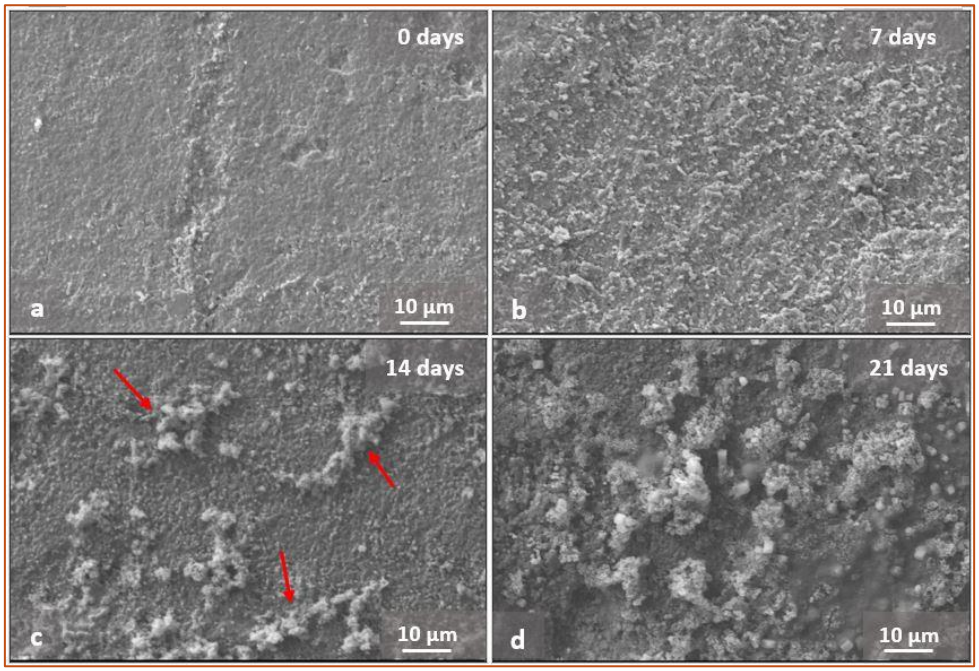

Figure 2. *Growth evolution of the coating on the surface of the samples during the biomimetic method: a) before coating (0 days), and after b) 7, c) 14, and d) 21 days of immersion coating. 3.00kx.*

Figure 3 illustrates the growth of the calcium phosphate layer within the pores during the biomimetic procedure, comparing samples before immersion (0 days) and after 7, 14, and 21 days of immersion. According to Figure 3b, after 7 days, phosphate formation inside pores was not evident in SEM images, but EDS analysis confirmed the deposition of calcium and phosphorous. By 14 days, cubic and spherical precipitates became visible in the SEM images. At 21, the amount of spherical calcium phosphate precipitates increased substantially, forming a uniform layer throughout the scaffolds, covering both the surface and the pores. The results within the pores present a resemblance to those on the surface.

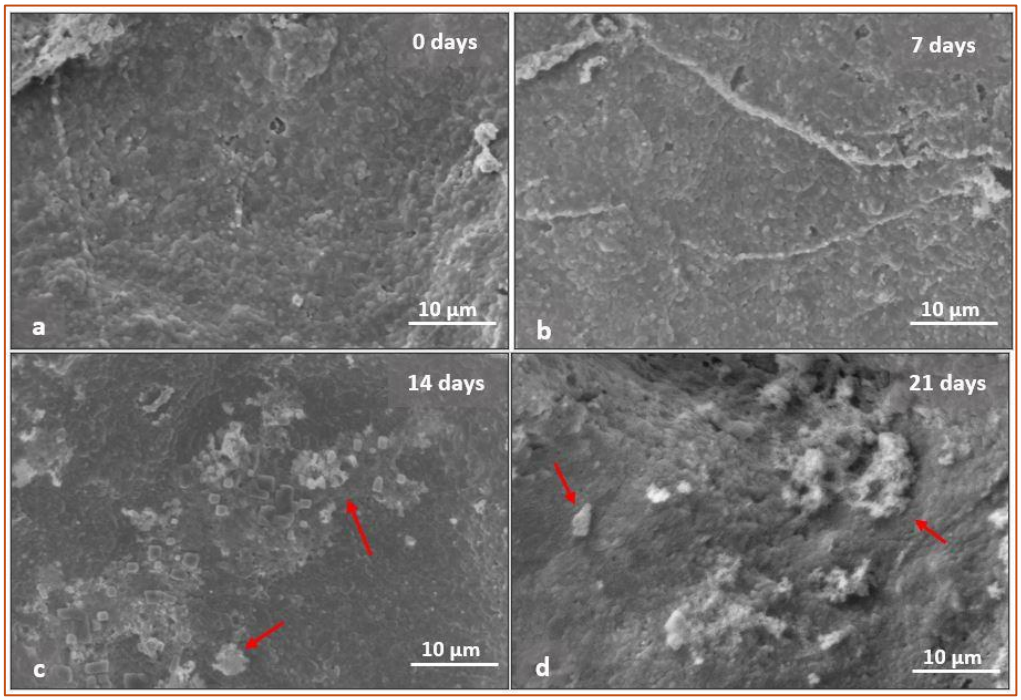

Figure 3*. Growth evolution of the coating during the biomimetic coating method on the surface of the pores: a) before immersion (0 days) and after b) 7, c) 14, and d) 21 days of immersion coating. 5.00kx.*

Calcium phosphates with cubic shapes observed in the samples align with a study on synthesizing calcium phosphate crystals with controlled size and shape, where these crystals were identified as dicalcium phosphate anhydrous (DCPA; $CaHPO_4$) [(29)]. Spherical shapes, as observed in Figures 2 and 3, are typical of hydroxyapatite (HAp; $Ca_{10}(PO_4)_6(OH)_2$) and tricalcium phosphate (α--TCP, β-TCP; $Ca_3(PO_4)_2$), which are the main phases expected after the biomimetic process [(3,23,26)]. It can be assumed that the calcium phosphate formed in the shorter immersion time is the precursor of the HAp and TCP phases identified in the 21-day sample. Sartori (2018) found similar behavior after 21 days of immersion and reported that the coating exhibited HAp, α-TCB, and β-TCP phases. More specifically, after 14 days, the coating consisted of 38% HAp and 62% TCP; after 21 days, the hydroxyapatite phase had increased to approximately 90%, with 10 TCP remaining[(18)].

Although SEM analysis (Figures 2 and 3) did not clearly show the formation of calcium phosphate after 7 days of immersion, this period may be sufficient to initiate the deposition of a calcium phosphate layer on the surface [(23,30-32)]. Figure 4 illustrates the small amount of these crystals deposited on the scaffolds at this stage. After 14 days of immersion, significant coverage of calcium and phosphorus was observed over almost the entire surface and within the pores (Figure 5), as observed in microscopy results [(22,23)]. By 21 days (Figure 6), calcium and phosphorus deposition were evident throughout the entire surface and pores, which suggests that the 21-day biomimetic procedure efficiently created a uniform coating across all scaffolds[(18,22,26)].

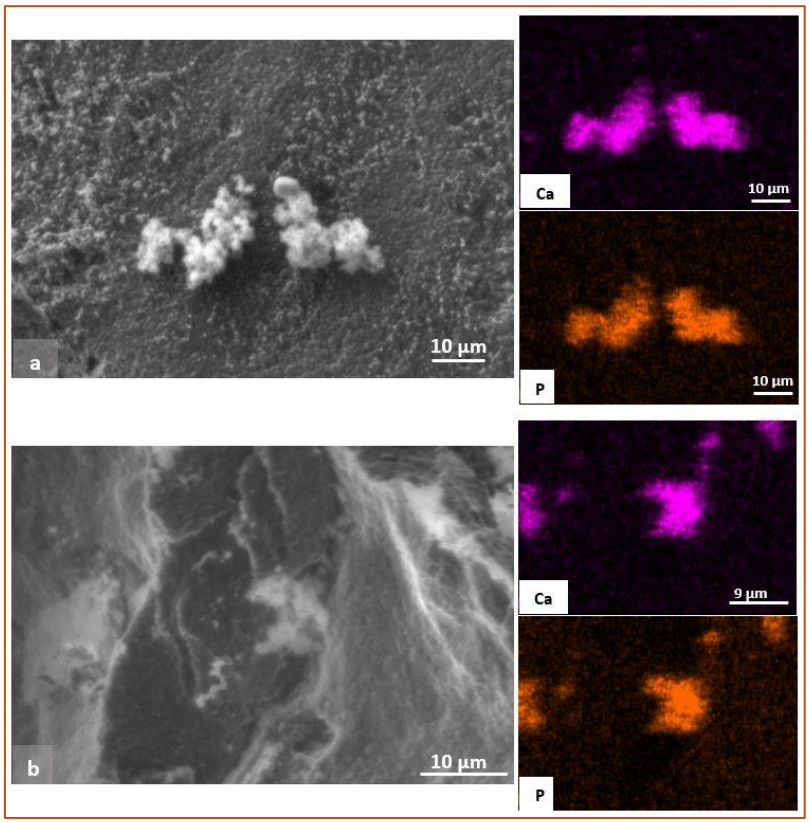

Figure 4. *EDS mapping after 7 days of immersion into the coating solution: (a) on the surface (3.00kx) and (b) within the pores. 5.00kx.*

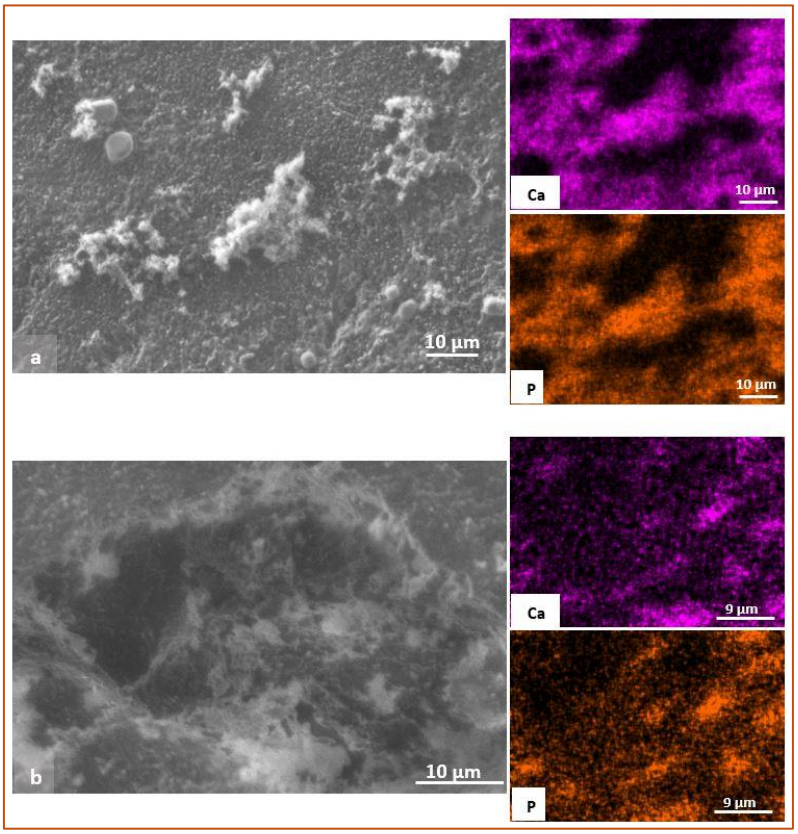

Figure 5. *EDS mapping after 14 days of immersion into the coating solution: (a) on the surface (3.00kx) and (b) within the pores. 5.00kx.*

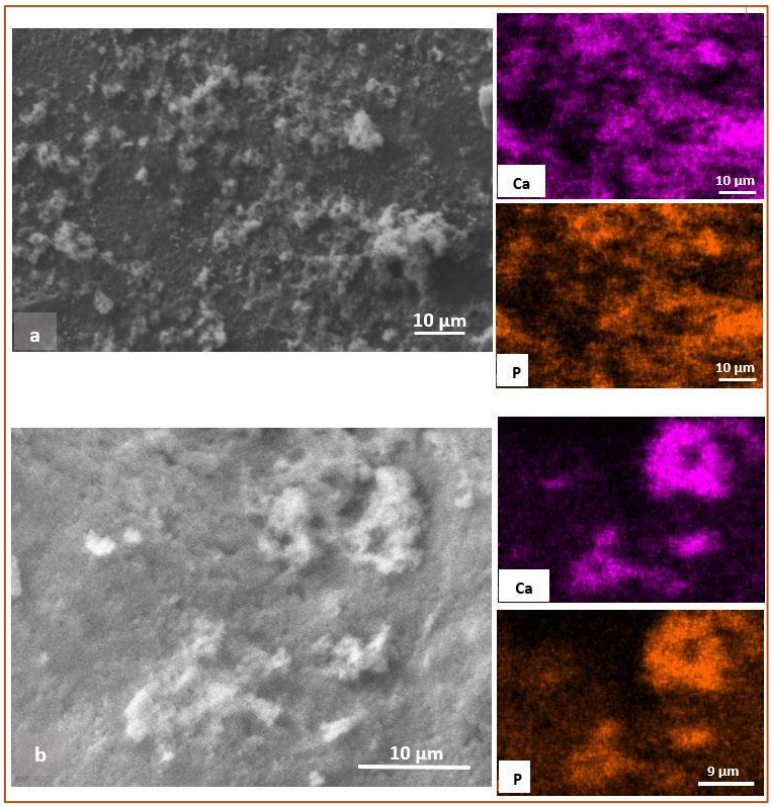

Figure 6. *EDS mapping after 21 days of immersion into the coating solution: (a) on the surface (3.00kx) and (b) within the pores. 5.00kx.*

The EDS maps at different immersion times showed the formation of a calcium phosphate layer under all conditions. The intensity of calcium and phosphorus present on the surfaces supports the presence of calcium phosphate phases with different morphologies in the coating. The EDS results allowed the evaluation of the Ca/P ratio (Table 3), which is typical for each calcium phosphate phase. The expected Ca/P values after biomimetic coating are close to TTCP (2.0), HAp (1.67), TCP (1.5), OCP (1.3), and DCPA (1.0).

Deb (2019) reported a coating with a Ca/P ratio of 1.55 after 28 days, which indicates the formation of Ca-deficient apatite [(28)]. Silva (2017) coated porous alumina and alumina/zirconia, finding Ca/P ratios between 1.75 and 2.20, with values closer to 1.75 at the end of the process [(34)]. Sartori (2018) observed Ca/P values of approximately 0.5 after 7 days, 1.43 and 1.31 after 14 days, similar to TCP and OCP, and 1.71 and 1.89 after 21 days, corresponding to HAp and TTCP [(18)]. Rambo (2006) achieved a homogenous calcium phosphate layer with a Ca/P ratio of 1.62[(23)]. Kim (2004) observed the formation of calcium phosphate with the same ratio, and these values tended to be 1.65 by 21 days[(35)].

Samples		Chemical elements (%atomic)		
		Ca	P	Ca/P ratio
7B	Surface	1.70	1.45	1.17
7B		0.85	0.50	1.70
14B		1.34	0.97	1.38
14B		3.52	2.88	1.22
21B		2.10	1.90	1.10
21B		4.44	2.94	1.51
7B	Within pores	1.22	0.63	1.93
7B		0.63	0.37	1.70
14B		0.88	0.66	1.33
14B		0.89	0.58	1.53
21B		3.34	2.38	1.40
21B		0.63	0.35	1.80

Table 3. *EDS results after biomimetic coating, with Ca/P ratios.*

During the biomimetic coating process, different phases of calcium phosphate can form. By the end of the procedure, the coating layer was expected to predominantly consist of HAp (Ca/P = 1.67) and TCP (Ca/P = 1.5). Surface pores can act as defects that enhance the nucleation and growth of calcium phosphate crystals. The roughness variation and the induction of surface defects caused by the sanding procedure likely increased the contact area between the scaffold surface and the simplified solution (SS), which is beneficial for crystal formation[22].

Figure 7 shows the X-ray diffraction XRD results on scaffolds before (0B) and after (7B, 14B, 21B) the biomimetic process. XRD spectra showed no evidence of a calcium phosphate layer on the surface after the biomimetic process, as similar patterns were observed for all conditions: uncoated (0b), 7 days, 14, and 21 days of immersion into the coating solution. This apparent absence of calcium phosphate may be attributed to the nanometric thickness of the coating layer or the presence of amorphous phases. Despite the lack of XRD detection, the SEM results confirmed the formation of a calcium phosphate layer formation on the surfaces of all samples.

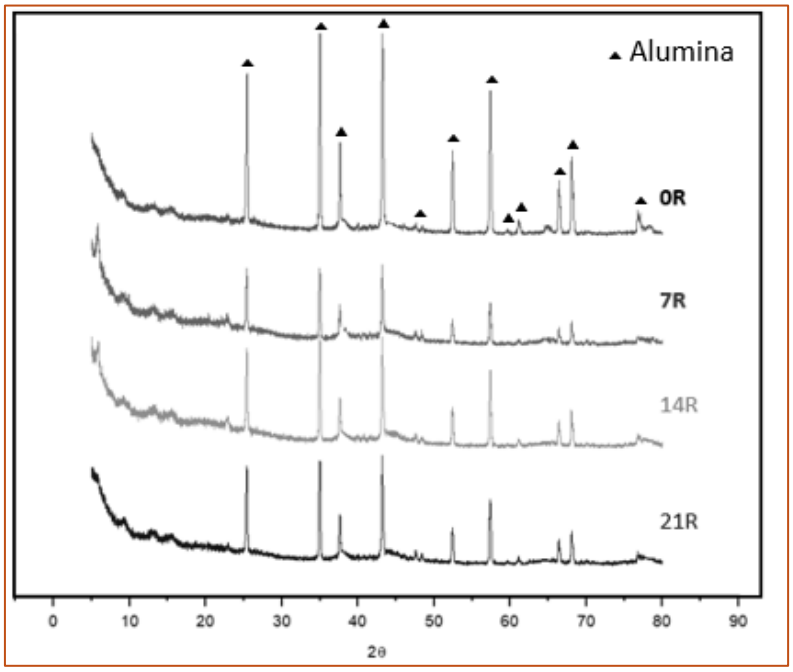

Figure 7. *X-ray diffraction on scaffolds before and after coating.*

Figure 8 presents the FTIR spectra of the samples before (0B) and after (7B, 14B, and 21B) the biomimetic procedure. The PO_4^{3-} groups were identified at various vibration frequencies. Peaks observed in the spectra were 461 cm^{-1}, 607 cm^{-1}, 656 cm^{-1}, 789 cm^{-1}, 1082 cm^{-1} and 3335 $cm^{-1,}$ as indicated in Figure 8. The doubly degenerated vibrational mode of the O-P-O group can be identified at ~ 461 cm^{-1} (v_2), while a peak at 789 cm^{-1} (v_1) was assigned to the O-P-O group. The triply degenerated bend mode of the P-O group was observed at ~ 656 cm^{-1} (v_1) and 1082 cm^{-1} (v_3). A peak at ~3300 cm^{-1} corresponds to the OH- band (v_3, v_4)[24,36].

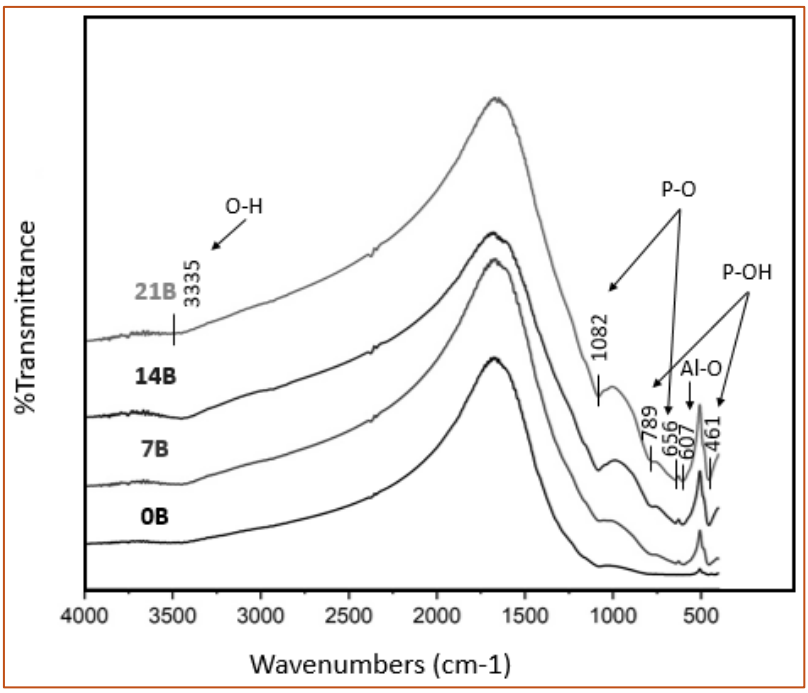

Figure 8. *Infrared transmittance spectra of scaffolds before and after biomimetic coating.*

All samples presented characteristic vibrational groups of calcium phosphates and hydroxyl. These results support the hypothesis that a CaP layer forms on the scaffold surfaces after immersion into the coating solution, confirming the deposition of the biomimetic coating.

CONCLUSIONS

The powder metallurgy method was effective in fabricating alumina scaffolds, achieving a porosity of 55% with 40 wt.% NH_2CO_3. Heat treatment at 270 °C for 120 min efficiently removed NH_2CO_3. After 7 days of biomimetic coating, the initial formation of a CaP layer was observed. The procedure effectively supported the formation of multiple calcium phosphate phases, with a greater concentration of Hap and TCP detected after 21 days. Additionally, CaP was observed across the surfaces, both externally and within the pores. SEM, EDS mapping, and Ca/P ratio results strongly indicated the presence of these calcium phosphate phases.

Declaración de financiamiento:	Los autores agradecen al Sistema Nacional de Laboratorios de Nanotecnología (MCTI/SisNANO/INT-CENANO-CNPq Número de proceso 442604/2019-0) y CAPES por el apoyo financiero. La Dra. Ana Paula Luz y FAI UFSCar son responsables de la donación de alúmina.
Declaración de conflicto de intereses:	Los autores declaran que no existe conflicto de intereses.
Declaración de autores:	Los autores aprueban la versión final del artículo

REFERENCES

1. Winkler T, Sass FA, Duda GN, Schmidt-Bleek K. A review of biomaterials in bone defect healing, remaining shortcomings and future opportunities for bone tissue engineering: The unsolved challenge. Bone & Joint Research. 2018;7(3):232-43. Disponible en: 10.1302/2046-3758.73.BJR-2017-0270.R1
2. Barnsley J, Buckland G, Chan PE, Ong A, Ramos AS, Baxter M, et al. Pathophysiology and treatment of osteoporosis: challenges for clinical practice in older people. Aging Clin Exp Res. 2021;33(4):759-73. Disponible en: https://link.springer.com/10.1007/s40520-021-01817-y
3. Ahmed MK, Ramadan R, Afifi M, Menazea AA. Au-doped carbonated hydroxyapatite sputtered on alumina scaffolds via pulsed laser deposition for biomedical applications. Journal of Materials Research and Technology. 2020;9(4):8854-66. Disponible en: 10.1016/j.jmrt.2020.06.006
4. Li Q, Chang B, Dong H, Liu X. Functional microspheres for tissue regeneration. Bioactive Materials. 2023; 25:485-99. Disponible en: 10.1016/j.bioactmat.2022.07.025
5. Fernandes L, De Carvalho RA, Amaral AC, Pecoraro E, Salomão R, Trovatti E. Mullite cytotoxicity and cell adhesion studies. Journal of Materials Research and Technology. 2019; 8(3):2565–2572. Doi: 10.1016/j.jmrt.2019.04.001
6. Fernandes JS, Gentile P, Pires RA, Reis RL, Hatton PV. Multifunctional bioactive glass and glass-ceramic biomaterials with antibacterial properties for repair and regeneration of bone tissue. Acta Biomaterials. 2017;59:2–11. Disponible en: 10.1016/j.actbio.2017.06.046
7. Coelho CC, Padrao T, Costa L, et al. The antibacterial and angiogenic effect of magnesium oxide in a hydroxyapatite bone substitute. Scientific Reports. 2020; 10(1):19098. Doi: 10.1038/s41598-020-76063-9
8. Niu Y, Du T, Liu Y. Biomechanical Characteristics and Analysis Approaches of Bone and Bone Substitute Materials. Journal Functional Biomaterials. 2023; 14(4):212. Disponible en: 10.3390/jfb14040212
9. Coelho CC, Araújo R, Quadros PA, Sousa SR, Monteiro FJ. Antibacterial bone substitute of hydroxyapatite and magnesium oxide to prevent dental and orthopedic infections. Materials Science and Engineering C. 2019;97:529–538. Disponible en: 10.1016/j.msec.2018.12.059
10. Liu D, Liu Z, Zou J, et al. Synthesis and Characterization of a Hydroxyapatite-Sodium Alginate-Chitosan Scaffold for Bone Regeneration. Frontiers in Materials. 2021; 8:648980. Disponible en: 10.3389/fmats.2021.648980
11. Fan X. Preparation and performance of hydroxyapatite/Ti porous biocomposite scaffolds. Ceramics International. 2019;45(13):16466–16469. Disponible en: 10.1016/j.ceramint.2019.05.178
12. Mahmoodiyan Najafabadi F, Karbasi S, Zamanlui Benisi S, Shojaei S, Poursamar SA, Nasr Azadani R, Evaluation of the effects of alumina nanowire on 3D printed polycaprolactone/magnetic mesoporous bioactive glass scaffold for bone tissue engineering applications. Materials Chemistry and Physics. 2023;303: 127616. Disponible en: 10.1016/j.matchemphys.2023.127616
13. Ghafari F, Karbasi S, Eslaminejad MB. Investigating of physical, mechanical, and biological properties of polyhydroxybutyrate-keratin/alumina electrospun scaffold utilized in bone tissue engineering. Materials Chemistry and Physics. 2023;297:127340. Disponible en: 10.1016/j.matchemphys.2023.127340
14. Kim JM, Son JS, Kang SS, Kim G, Choi SH. Bone regeneration of hydroxyapatite/alumina bilayered scaffold with 3 mm passage-like medullary canal in canine tibia model. BioMed Research International. 2015:1-6. Disponible en: 10.1155/2015/235108
15. Anita Lett J, Sundareswari M, Ravichandran K. Porous hydroxyapatite scaffolds for orthopedic and dental applications-the role of binders. In Materials Today: Proceedings. 2016;3(6):1672-1677. Disponible en: 10.1016/j.matpr.2016.04.058
16. Feng S, He F, Ye J. Fabrication and characterization of honeycomb β-tricalcium phosphate scaffolds through an extrusion technique. Ceramics International. 2017;43(9):6778–6785. Disponible en: 10.1016/j.ceramint.2017.02.094
17. Ren X, Tuo Q, TianK, et al. Enhancement of osteogenesis using a novel porous hydroxyapatite scaffold in vivo and vitro. Ceramics International. 2018;44(17):21656–21665. Disponible en: 10.1016/j.ceramint.2018.08.249
18. Sartori TAI, Ferreira JA, Osiro D, Colnago LA, Agnolon Pallone EMJ. Formation of different calcium phosphate phases on the surface of porous Al2O3-ZrO2 nanocomposites. Journal of the European Ceramic Society. 2018; 38:743–751. Disponible en: 10.1016/j.jeurceramsoc.2017.09.014
19. Camilo CC. Implantes de alumina em gradiente funcional de porosidade recobertos com hidroxiapatita e biovidro: avaliação da osseointegração. Escola de Engenharia de São Carlos da Universidade de São Paulo, 2010.
20. Abe Y, Kokubo T, Yamamuro T. Apatite coating on ceramics, metals, and polymers utilizing a biological process. Journal of Materials Science: Materials in Medicine. 1990; 1:233–238. Disponible en: doi.org/10.1007/BF00701082
21. Gu Y, Liu Y, Jacobs R, et al. BMP-2 incorporated into a biomimetic coating on 3D-printed titanium scaffold promotes mandibular bicortical bone formation in a beagle dog model. Materials & Design. 2023;228:111849. Disponible en: 10.1016/j.matdes.2023.111849

22. Dos Santos KH, Ferreira JA, Osiro D, Da Conceição GJA, Filho RB, Colnago LA, et al. Influence of different chemical treatments on the surface of Al2O3/ZrO2 nanocomposites during biomimetic coating. Ceramics International. 2017;43(5):4272-9. Disponible en: 10.1016/j.ceramint.2016.12.069
23. Rambo CR, Müller FA, Müller L, Sieber H, Hofmann I, Greil P. Biomimetic apatite coating on biomorphous alumina scaffolds. Materials Science and Engineering C. 2006;26(1):92–99. Disponible en: 10.1016/j.msec.2005.06.003
24. Zafar B, Mottaghitalab F, Shahosseini Z, Negahdari B, Farokhi M. Silk fibroin/alumina nanoparticle scaffold using for osteogenic differentiation of rabbit adipose-derived stem cells. Materialia. 2020; 9:100518. Disponible en: 10.1016/j.mtla.2019.100518
25. Zhou X, Guan C, Ma Q, et al. Elaboration and characterization of ε-polylysine-sodium alginate nanoparticles for sustained antimicrobial activity. International Journal Biological Macromolecules. 2023;251(1):126329. Disponible en: 10.1016/j.ijbiomac.2023.126329
26. Costa HS, Mansur AAP, Barbosa-Stancioli IF, Pereira MM, Mansur HS. Morphological, mechanical, and biocompatibility characterization of macroporous alumina scaffolds coated with calcium phosphate/PVA. In Journal of Materials Science. 2008;43:510–524. Disponible en: 10.1007/s10853-007-1849-6
27. Duraccio D, Strongone V, Malucelli G, et al. The role of alumina-zirconia loading on the mechanical and biological properties of UHMWPE for biomedical applications. Composites Part B: Engineering. 2019;164(1):800–808. Disponible en: 10.1016/j.compositesb.2019.01.097
28. Deb P, Barua E, Deoghare AB, Das Lala S. Development of bone scaffold using Puntius conchonius fish scale derived hydroxyapatite: Physico-mechanical and bioactivity evaluations. Ceramics International. 2019;45(8):10004–10012. Disponible en: 10.1016/j.ceramint.2019.02.044
29. Lin K, Wu C, Chang J. Advances in synthesis of calcium phosphate crystals with controlled size and shape. Acta Biomaterialia. 2014;10(10):4071-4102. Disponible en: 10.1016/j.actbio.2014.06.017
30. Toloue EB, Karbasi S, Salehi H, Rafienia M. Potential of an electrospun composite scaffold of poly (3-hydroxybutyrate)-chitosan/alumina nanowires in bone tissue engineering applications. Materials Science and Engineering C. 2019;99:1075–1091. Disponible en: 10.1016/j.msec.2019.02.062
31. El-Mehalawy N, Sayed M, Abou El-Anwar EA, Soliman AAF, Naga SM. Preparation and characterization of bioceramic composites based on anorthite and β-TCP from dolomitic phosphate and kaolin rocks. Materials Chemistry and Physics. 2024;312(15): 128625. Disponible en: 10.1016/j.matchemphys.2023.128625
32. Oliveira IR, Goncalves IS, dos Santos KW, et al. Biocomposite Macrospheres Based on Strontium-Bioactive Glass for Application as Bone Fillers. ACS Materials Au. 2023;3(6):646-658. Disponible en: 10.1021/acsmaterialsau.3c00048
33. Pinto E Souz IE, De Carvalho SM, Martins T, De Magalhães Pereira M. Fluorine-containing bioactive glass spherical particles synthesized by sol-gel route assisted by ultrasound energy or mechanical mixing. Materials Research. 2020;23(3):16–19. Disponible en: 10.1590/1980-5373-MR-2020-0070
34. Silva JC. Desenvolvimento de carreadores lipídicos nanoestruturados como sistema de carreamento de extrato de Cúrcuma longa e avaliação biológica in vitro em células de câncer de bexiga. Master, Faculdade de Ciências Farmacêuticas de Ribeirão Preto da Universidade de São Paulo, 2017.
35. Kim HM, Himeno T, Kawashita M, Kokubo T, Nakamura T. The mechanism of biomineralization of bone-like apatite on synthetic hydroxyapatite: An in vitro assessment. Journal of the Royal Society Interface.2004;1(1):17–22. Disponible en: 10.1098/rsif.2004.0003
36. Mondal S, Hoang G, Manicasagan P, et al. Nano-hydroxyapatite bioactive glass composite scaffold with enhanced mechanical and biological performance for tissue engineering application. Ceramics International. 2018;44(13):15735–15746. Disponible en: 10.1016/j.ceramint.2018.05.248